Article

Nanoscale Assembly of CdS/BiVO$_4$ Hybrids for Coupling Selective Fine Chemical Synthesis and Hydrogen Production under Visible Light

Feng-Kang Shang, Ming-Yu Qi, Chang-Long Tan, Zi-Rong Tang,* and Yi-Jun Xu*

Cite This: *ACS Phys. Chem Au* 2022, 2, 216−224

Read Online

ACCESS | Metrics & More | Article Recommendations | SI Supporting Information

ABSTRACT: Simultaneously utilizing photogenerated electrons and holes in one photocatalytic system to synthesize value-added chemicals and clean hydrogen (H$_2$) energy meets the development requirements of green chemistry. Herein, we report a binary material of CdS/BiVO$_4$ combining one-dimensional (1D) CdS nanorods (NRs) with two-dimensional (2D) BiVO$_4$ nanosheets (NSs) constructed through a facile electrostatic self-assembly procedure for the selectively photocatalytic oxidation of aromatic alcohols integrated with H$_2$ production, which exhibits significantly enhanced photocatalytic performance. Within 2 h, the conversion of aromatic alcohols over CdS/BiVO$_4$-25 was approximately 9-fold and 40-fold higher than that over pure CdS and BiVO$_4$, respectively. The remarkably improved photoactivity of CdS/BiVO$_4$ hybrids is mainly ascribed to the Z-scheme charge separation mechanism in the 1D/2D heterostructure derived from the interface contact between CdS and BiVO$_4$, which not only facilitates the separation and transfer of charge carriers, but also maintains the strong reducibility of photogenerated electrons and strong oxidizability of photogenerated holes. It is anticipated that this work will further stimulate interest in the rational design of 1D/2D Z-scheme heterostructure photocatalysts for the selective fine chemical synthesis integrated with H$_2$ evolution.

KEYWORDS: CdS, BiVO$_4$, hydrogen evolution, aromatic alcohols oxidation, photoredox dual reaction
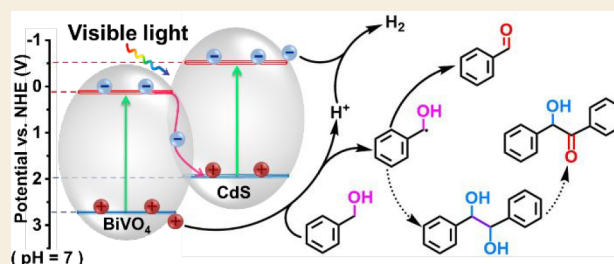
1. INTRODUCTION

As ubiquitous intermediates for the production of many fine chemicals and pharmaceuticals, aromatic carbonyl compounds are of great significance in the industries of perfumes, dyes, and medicines.[1] Aromatic carbonyl compounds can be directly obtained by selective transformation of aromatic alcohols, which is considered to be one of the most vital reactions in organic synthesis.[2] As the simplest aromatic aldehyde with an active carbonyl group, benzaldehyde (BAD) occupies an essential position in organic reaction intermediates.[3,4] The traditional industrial way to synthesize BAD is liquid toluene oxidation or benzoyl chloride hydrolysis, which not only generates various byproducts (bromobenzene, etc.), but also brings about severe environmental pollution and energy waste.[5,6] In this context, solar-driven oxidation of benzyl alcohol (BA) has attracted more attention due to its advantages of benign environmental impact and low energy consumption.[7−10] Most of the various researches on photocatalytic alcohols oxidation choose oxygen (O$_2$) as the electron acceptor.[7,11,12] In comparison, direct splitting of alcohols into hydrogen (H$_2$) and corresponding carbonyl products not only makes full use of the energy of photoinduced electron−hole pairs, but also produces clean H$_2$ fuels, thereby offering a cooperative photoredox reaction system.[13,14] Accordingly, photocatalytic selective conversion of BA at

ambient conditions coupling with protons reduction to produce H$_2$ is a promising alternative.[15−24]

The monoclinic scheelite phase BiVO$_4$ is a typical semiconductor with many advantages, including visible light response, suitable valence band (VB) position, good stability, extensive sources of its constituent elements, and mild environmental impact.[25] Therefore, it is widely reported that the BiVO$_4$ nanomaterials with various morphologies have been prepared and utilized in the research of photocatalytic alcohols conversion.[26−28] Among them, benefiting from the large specific surface area and short carrier transport distance, ultrathin two-dimensional (2D) BiVO$_4$ nanosheets (NSs) with several atomic layer thicknesses show excellent performance in heterogeneous photocatalysis.[21,29,30] However, pure BiVO$_4$ still has limitations: on the one hand, the rapid recombination of photoexcited electron−hole pairs severely limits the photoactivity of BiVO$_4$; on the other hand, the conduction band (CB) is so positive that

the electrons in it are difficult to use or transfer.[25] Some strategies have been developed to overcome the aforementioned shortcomings, such as morphological control, loading cocatalysts, doping impurity, and designing type-II heterostructure composites. These methods can improve the shortcomings of low photogenerated carriers transport and separation efficiency, but cannot change the fact that the energy of the photogenerated electrons is not sufficient to reduce hydrogen protons.[20,31−34] In comparison, designing composite materials with a Z-scheme charge transfer pathway is a feasible solution to achieve this goal for the photoexcited electrons and holes gathering in a more negative CB and a more positive VB, respectively, thereby retaining strong photoredox properties.[29,30,35−38]

Among various semiconductors that can form a Z-scheme system with $BiVO_4$, CdS is one of the most promising candidates due to its suitable band gap and ideal position of CB for H_2 production.[39,40] Thereinto, one-dimensional (1D) CdS nanorods (NRs) exhibit excellent photocatalytic performance for H_2 evolution, which is attributed to the high aspect ratio and single crystal with high crystallinity favoring the migration and separation of charge carriers.[41,42] However, the applications of pure CdS NRs are severely limited due to the shortcomings of CdS, such as photocorrosion and rapid recombination of photogenerated carriers, which can be effectively solved by constructing a Z-scheme system.[6,43−45] The CdS/$BiVO_4$ binary system has been reported for dye degradation,[30] CO_2 reduction,[29] H_2 evolution,[37] and conversion of biomass derivatives,[38] but the selective transformation of photocatalytic biomass derivatives (e.g., alcohols) integrated with H_2 production in one photoredox cycle over CdS/$BiVO_4$ hybrids is still reported scarcely.

In this work, we have successfully constructed a CdS/$BiVO_4$ 1D/2D binary nanocomposite through a facile one-step electrostatic self-assembly method for coproduction of H_2 and BAD under visible light illumination ($\lambda > 420$ nm), utilizing photoinduced electrons and holes simultaneously. A direct Z-scheme heterostructure can be formed between CdS NRs and $BiVO_4$ NSs motivated by the substantial electrostatic attraction between CdS with a positive charge and $BiVO_4$ with a negative charge, which can effectively promote the migration and separation of photoexcited electron−hole pairs.[46] As expected, compared with bare CdS and $BiVO_4$, the as-prepared CdS/$BiVO_4$ hybrids display significantly enhanced photoactivity toward visible light-driven splitting of BA into BAD and H_2. Particularly, the ratios of reduction product (H_2) and oxidation products are calculated to be 1:1, approximately, indicating that a visible light-driven alcohol dehydrogenation reaction in a stoichiometric manner is realized in our system. It is hoped that this study could open up a new horizon for developing collaborative photoredox systems of 1D/2D composite materials with a Z-scheme heterostructure, thereby realizing low-cost and high-efficiency conversion of biomass derivatives and production of green energy.

2. EXPERIMENTAL SECTION

2.1. Materials

Ammonium metavanadate (NH_4VO_3), sodium hydroxide (NaOH), bismuth(III) nitrate pentahydrate ($Bi(NO_3)_3 \cdot 5H_2O$), thiourea (H_2CNSNH_2), nitric acid (HNO_3), ethylenediamine ($C_2H_8N_2$), dimethyl sulfoxide (C_2H_6OS, DMSO), *tert*-butyl alcohol ($C_4H_{10}O$, ^tBuOH), ethanol (EtOH), methyl cyanide (MeCN), carbon tetrachloride (CCl_4), and triethanolamine (TEOA) were supplied by Sinopharm Chemical Reagent Co., Ltd. (Shanghai, China). 5,5-

Dimethyl-1-pyrroline-*N*-oxide (DMPO), sodium dodecylbenzenesulfonate ($C_{18}H_{29}NaO_3S$, SDBS), and cadmium nitrate tetrahydrate ($CdN_2O_6 \cdot 4H_2O$) were purchased from Aladdin Biochemical Technology Co., Ltd. (Shanghai, China). All reagents are utilized without further purification. Deionized (DI) water utilized in all the experiments comes from local sources.

2.2. Synthesis Method

2.2.1. Synthesis of $BiVO_4$ Nanosheets (NSs). The $BiVO_4$ NSs were synthesized via a hydrothermal method according to a literature procedure, which went through a few modifications.[29,30] The typical experimental procedure is provided in the Supporting Information.

2.2.2. Synthesis of CdS Nanorods (NRs). The CdS NRs were prepared via a solvothermal process according to a literature procedure.[47,48] The typical experimental procedure is provided in the Supporting Information.

2.2.3. Preparation of CdS/$BiVO_4$ Hybrids. Typically, the positively charged CdS NRs (100 mg) and the negatively charged $BiVO_4$ NSs (a certain amount) were first dispersed into DI water (50 and 10 mL, respectively) by sonication for 0.5 h. Then, the CdS NRs suspension and $BiVO_4$ NSs suspension were mixed and stirred vigorously for 1 h. Afterward, the resultant samples were collected via suction filtration, rinsed with DI water for several times, and dried in an oven for 6 h. The added weight amounts of $BiVO_4$ NSs in the CdS/$BiVO_4$ hybrids (CdS/$BiVO_4$-X, X = 15, 20, 25, 30 and 35) were controlled to be 15, 20, 25, 30, and 35 wt % of CdS NRs, respectively.

2.3. Photocatalytic Conversion of BA

The photocatalytic splitting of BA into BAD and H_2 was carried out in a single-walled quartz Schlenk tube. In a typical process, 0.1 mmol BA and 5 mg of photocatalyst were mixed into the quartz reactor prefilled with 5 mL of MeCN. Before irradiation, the reaction suspension was sonicated for 2 min to form a uniform suspension and degassed with nitrogen for 30 min to purge air. Subsequently, a 300 W Xe lamp (PLS-SXE 300D, Beijing Perfectlight Co., Ltd.) emitting visible light ($\lambda > 420$ nm) was used as the irradiation source to trigger the photocatalytic reaction. The energy output of the Xe lamp was measured to be 0.8 W cm^{-2} by a photoradiometer (PL-MW2000, Beijing Perfectlight Co., Ltd.). The operating conditions of the control experiments or extended experiments were the same as the above-mentioned photocatalytic process except for the controlled reaction conditions. The operation of the cycling tests is as follows. After the photocatalytic reaction is completed, the used photocatalyst is separated by centrifugation, washed with DI water, dried in a vacuum oven, and then utilized for the next activity test, which is repeated five times. After the reaction, the gas chromatograph (Shimadzu GC-2014C, MS-5 A column, TCD, Ar carrier) was utilized to quantitatively detect the gases products. After that, the suspension was filtered through a Nylon syringe filter (0.22 μm) to obtain a clear solution, which was qualitatively analyzed by gas chromatograph−mass spectrometer (Shimadzu GC-MS QP 2020, Q-Exactive) and quantitatively detected by a high-performance liquid chromatograph (Shimadzu HPLC-LC20AT, C18 column, SPD-M20A). The conversion of BA and selectivity of each oxidation product were calculated with the following equations:[13,16]

$$\text{conversion of BA \%} = \frac{n_0 - n_{BA}}{n_0} 100$$

$$\text{selectivity for BAD \%} = \frac{n_{BAD}}{n_{BAD} + n_{C-C}} 100$$

$$\text{selectivity for C−C products \%} = \frac{n_{C-C}}{n_{BAD} + n_{C-C}} 100$$

where n_0 represents the amount of BA that was added into the system initially; n_{BA} represents the amounts of the residual BA; n_{BAD} and n_{C-C}, respectively, stand for the amounts of BAD and C−C products after reacting for a certain time.
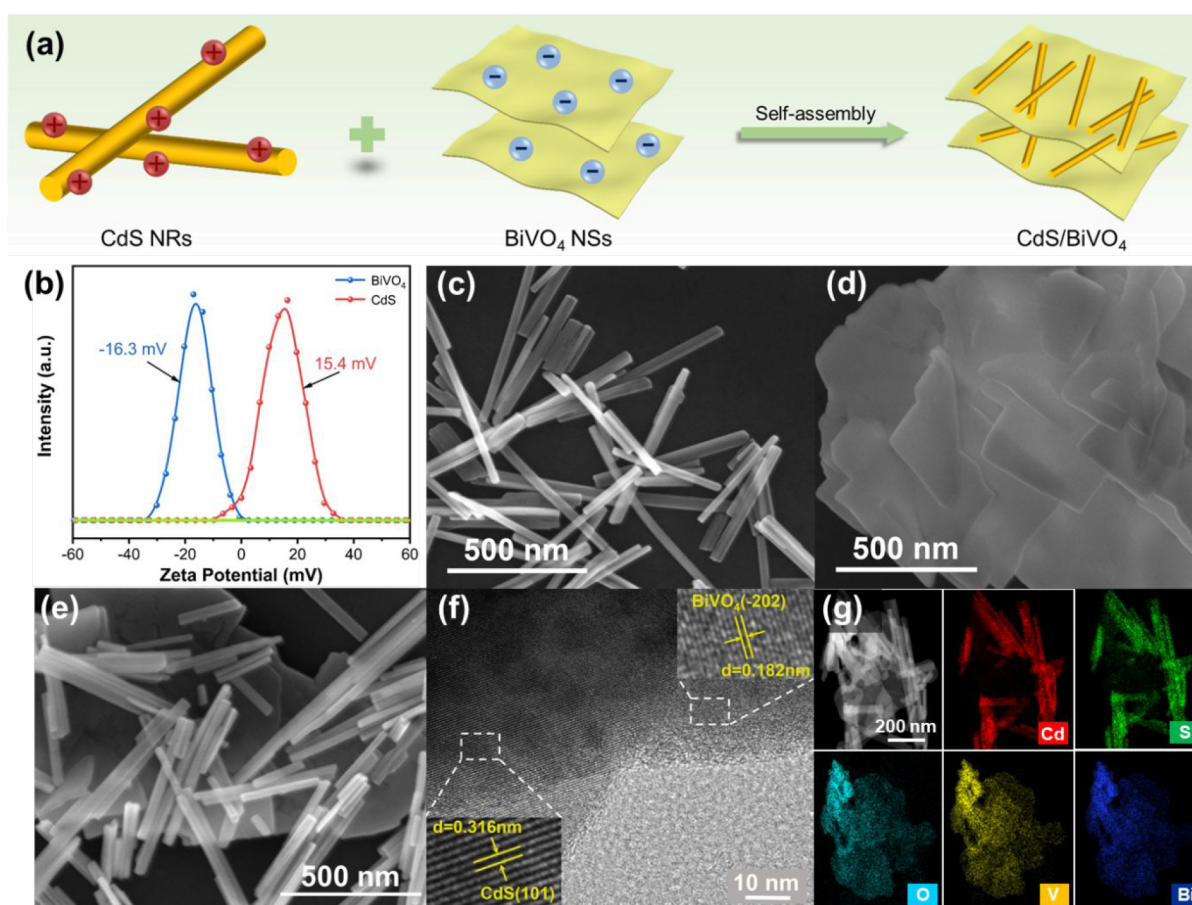
Figure 1. (a) Schematic illustration of the fabrication of CdS/BiVO$_4$ hybrids. (b) Zeta potentials of the as-synthesized CdS NRs and BiVO$_4$ NSs. FESEM images of (c) CdS NRs, (d) BiVO$_4$ NSs, and (e) CdS/BiVO$_4$ hybrids. (f) HRTEM image of CdS/BiVO$_4$ hybrids, in which the inset is the magnification of the image displayed in the panel surrounded by white dotted lines. (g) Corresponding elemental mapping images of CdS/BiVO$_4$ hybrids.

3. RESULT AND DISCUSSION

The CdS/BiVO$_4$ 1D/2D hybrids are fabricated via a nanoscale self-assembly methodology, as depicted in Figure 1a. Initially, bare CdS NRs and BiVO$_4$ NSs are synthesized through a solvothermal process, and their surface charge properties are ascertained by zeta potential measurements.[30,48] As illustrated in Figure 1b, the surface of the BiVO$_4$ NSs is obvious negatively charged (the zeta potential value is −16.3 mV), while CdS NRs exhibit positively charged (the zeta potential value is 15.4 mV) by reason of the residual amino ions.[49,50] Consequently, the electrostatic interaction between CdS NRs and BiVO$_4$ NSs allows the spontaneous formation of CdS/BiVO$_4$ 1D/2D heterostructure through electrostatic self-assembly strategy.[38] The morphological characteristics of different samples are observed by field emission scanning electron microscope (FESEM). As illustrated in Figure 1c,d, the bare CdS has significant 1D nanorod morphology with an average diameter distribution of about 40−80 nm, while the bare BiVO$_4$ manifests legible ultrathin 2D NSs, the thickness of which is about 30−50 nm. Figure 1e clearly shows that CdS NRs and BiVO$_4$ NSs form a 1D/2D morphology with good interface contact through electrostatic interaction. After that, high resolution transmission electron microscope (HRTEM) characterizations have been further conducted to gain insight into the microstructure information of CdS/BiVO$_4$ hybrids. As observed in Figure 1f, the 0.316 and 0.182 nm lattice fringes respectively correspond to

the (101) facet of CdS and the (−202) facet of monoclinic BiVO$_4$. Energy-dispersive X-ray spectroscopy (EDX) and element mapping have been carried out to determine the elements composition and distribution. The EDX spectrum plotted in Figure S1 ascertains the existence of Cd, S, Bi, V, and O in the composite material. Besides, the element mapping results illustrated in Figure 1g further demonstrate that CdS NRs are stacked well upon BiVO$_4$ NSs.

The crystal structure characteristics of a series of CdS/BiVO$_4$ hybrids have been probed via X-ray diffraction (XRD), as observed in Figure 2a. With regard to the composite samples, the peaks marked with red rounds are in agreement with the characteristic diffraction peaks of bare CdS, which can be indexed to hexagonal phase CdS (JCPDS No. 41-1049).[49,51] The peaks marked with black quadrilaterals are consistent with the characteristic diffraction peaks of bare BiVO$_4$ that can be indexed to monoclinic phase BiVO$_4$ (JCPDS No. 14-0688).[52] The diffraction peak intensities of BiVO$_4$ become stronger as the content of BiVO$_4$ NSs increases. Ultraviolet−visible diffuse reflectance spectroscopy (UV−vis DRS) was conducted to observe the optical absorption properties of the as-prepared samples. As mirrored in Figure 2b, all of the samples possess absorption bands in the visible light region from 450 to 550 nm. The absorption strength of the composite samples does not exhibit significant enhancement, suggesting that the formation of the 1D/2D heterostructure has no significant effect on the optical absorption of the composites. The band gap values of
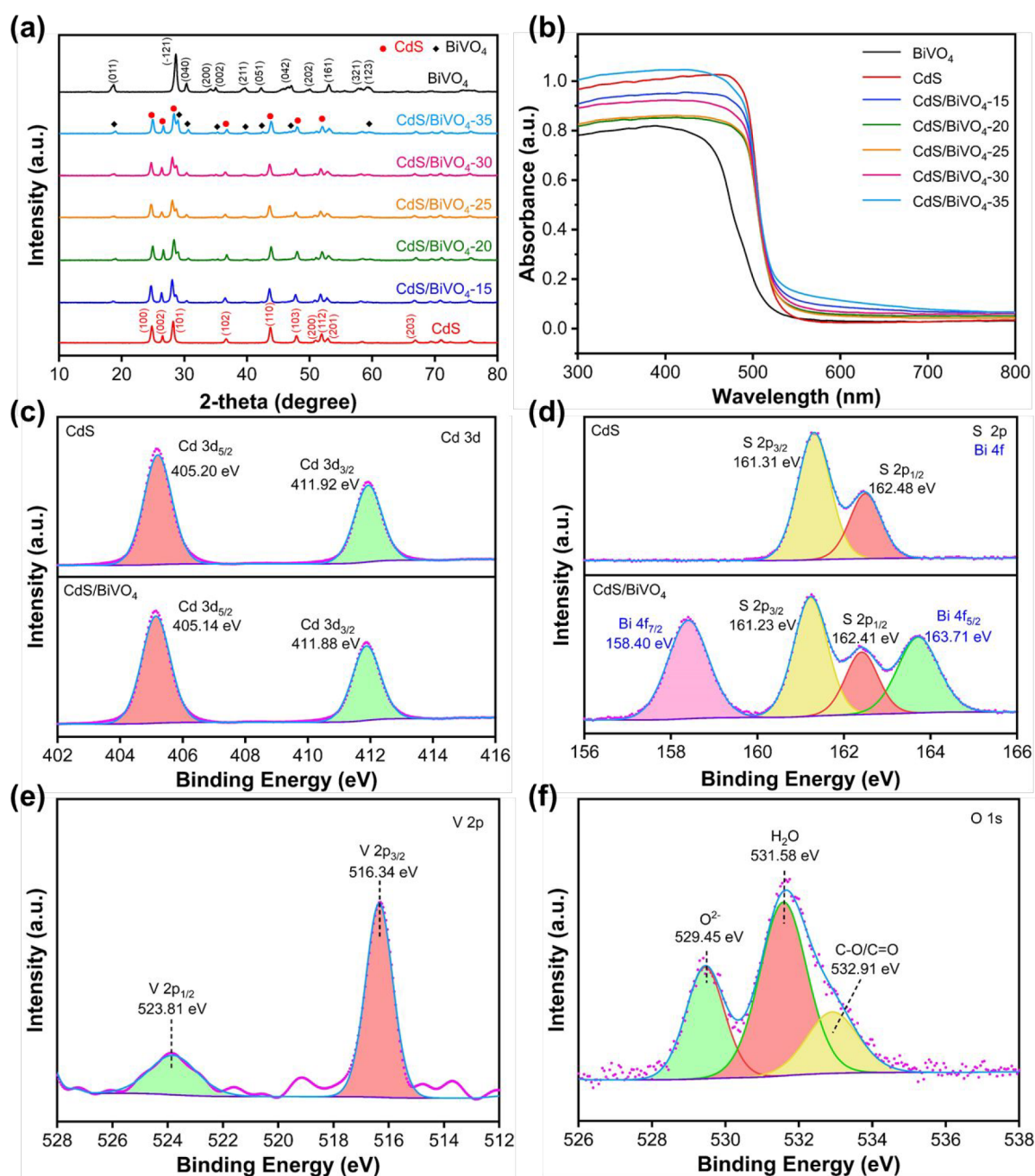
Figure 2. (a) XRD patterns of bare CdS NRs, BiVO$_4$ NSs, and a series of CdS/BiVO$_4$ hybrids with different weight ratios of BiVO$_4$ NSs. (b) UV−vis DRS spectra of blank CdS NRs, BiVO$_4$ NSs, and a series of CdS/BiVO$_4$ hybrids. High-resolution XPS spectra for (c) Cd 3d, (d) S 2p, and Bi 4f, (e) V 2p and (f) O 1s of the CdS/BiVO$_4$ hybrid.

CdS and BiVO$_4$ calculated according to the Kubelka−Munk function are respectively 2.42 and 2.53 eV (Figure S2), which means that they can be excited by visible light.[30] In addition, on the grounds of the Mott−Schottky curves (Figure S3), both the CdS and BiVO$_4$ exhibit the trends of n-type semiconductors, of which the flat band potentials are respectively situated in −0.70 and 0.00 V (vs Ag/AgCl). Since the conduction band (CB) positions of n-type semiconductors are close to their flat band potentials, the CB positions of CdS and BiVO$_4$ are respectively estimated at −0.50 and 0.20 V (vs NHE). Considering the band gap values obtained before, the valence band (VB) positions of CdS and BiVO$_4$ are respectively calculated to be 1.92 and 2.73 V

on the grounds of the formula $E_{VB} = E_{CB} + E_g$ (E_{VB}, E_{CB}, and E_g respectively are the energy values of VB, CB, and band gap).

X-ray photoelectron spectroscopy (XPS) has been utilized to deeply analyze the surface valence states of the chemical elements in the CdS/BiVO$_4$ hybrids. As displayed in the survey XPS spectrum of the CdS/BiVO$_4$ hybrid (Figure S4), all elements (Cd, S, Bi, V, and O) related to CdS and BiVO$_4$ are detected, which is consistent with the aforementioned EDX spectrum results. The two peaks of 405.14 and 411.88 eV depicted in the Cd 3d spectrum (Figure 2c) are respectively ascribed to Cd 3d$_{5/2}$ and Cd 3d$_{3/2}$, corresponding to Cd^{2+}.[53] In Figure 2d, the two peaks with binding energies of 161.23 and
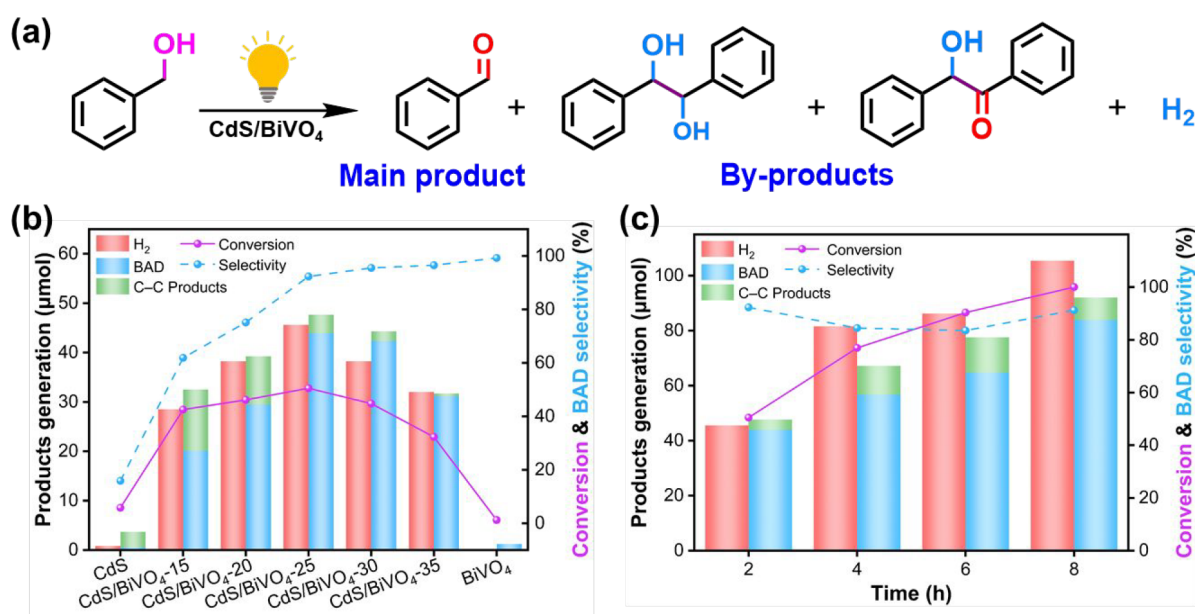
Figure 3. (a) Formula for photoredox reaction coupling BA oxidation and H_2 evolution. (b) Results of photocatalytic measurements for selective conversion of BA over bare CdS, bare $BiVO_4$, and a series of $CdS/BiVO_4$ hybrids. (c) Long-time experiments over $CdS/BiVO_4$-25.

162.41 eV deconvoluted from the S 2p spectrum belong to S $2p_{3/2}$ and S $2p_{1/2}$, which can be ascribed to S^{2-}.[54] And the two peaks with binding energies of 158.40 and 163.71 eV are respectively attributed to Bi $4f_{7/2}$ and Bi $4f_{5/2}$, which proves the existence of Bi^{3+}.[55] The V 2p spectrum (Figure 2e) displays that the binding energies of V $2p_{3/2}$ and V $2p_{1/2}$ are respectively fixed at 516.34 and 523.81 eV, indicating the valence state of V is +5.[56] In Figure 2f, the O 1s spectrum can be deconvoluted into three peaks with binding energies of 532.91, 531.58, and 529.45 eV, which are in line with C−O/C=O, surface-adsorbed H_2O, and the lattice oxygen of layer-structured $Bi_2O_2^{2+}$, respectively.[57] All the above results further confirm that CdS and $BiVO_4$ have been successfully combined.

Subsequently, the selective oxidation of BA and the simultaneous H_2 production over the obtained samples were examined in the N_2 saturated acetonitrile solution under visible light irradiation (λ > 420 nm) (Figure 3a and Figure S5). As plotted in Figure 3b and Figure S6, both bare CdS and bare $BiVO_4$ show extremely low activity for the generation of BAD and H_2 because of the rapid recombination of photoexcited electrons and holes, even the H_2 evolution activity of $BiVO_4$ is negligible owing to its overpositive CB position. In contrast, the photoactivity of the $CdS/BiVO_4$ composite is significantly increased. Among them, $CdS/BiVO_4$-25 exhibits the strongest activity with the conversion of BA reaching 50.5% within 2 h (43.96 μmol for BAD and 45.58 μmol for H_2), which achieves about 9-fold and 40-fold improvement as compared to that for bare CdS and bare $BiVO_4$, respectively. Given that the oxidation ability of $BiVO_4$ is relatively strong with the products concentrated in BAD while the oxidation products of CdS tilt toward C−C coupled products due to the relatively mild oxidation ability of CdS, the selectivity of BAD increases as the content of $BiVO_4$ increases owing to the BA oxidation competing between CdS and $BiVO_4$. The selectivity of BAD has reached more than 90% when the $BiVO_4$ content is greater than 25%. To explore the relationship between light absorption and photoactivity, the calculated apparent quantum yield (AQY) of the $CdS/BiVO_4$-25 under different wavelengths of monochromatic light is measured and found to match

substantially with its DRS spectrum (Figure S7). A long-term reaction test and recycling experiment are conducted to assess the stability and reusability of $CdS/BiVO_4$ hybrids. As sketched in Figure 3c, after 8 h of exposure to visible light, the conversion of BA over $CdS/BiVO_4$-25 reaches 100%, with the selectivity of BAD as high as 91.2%. Additionally, $CdS/BiVO_4$-25 is not significantly inactivated after five cycles of testing (Figure S8), and its crystal structure also remains stable (Figure S9). The above results reveal the good stability of the $CdS/BiVO_4$ hybrids.

Aiming to further manifest the universality of $CdS/BiVO_4$ in the photocatalytic conversion of aromatic alcohols, we have carried out photocatalytic activity tests of diverse aromatic alcohols (1-phenethyl alcohol, p-methoxybenzyl alcohol, p-methylbenzyl alcohol, p-fluorobenzyl alcohol, and p-chlorobenzyl alcohol). As illustrated in Table S2, it is seen that the CdS/ $BiVO_4$ hybrid has varying degrees of photoactivity for the transformation of all aromatic alcohols, and the main products are the corresponding aromatic aldehydes or aromatic ketones. Notably, for benzylic alcohols with different substituents, the introduction of electron-donating groups on the benzene ring significantly enhances the conversion rate of aromatic alcohols. For instance, the conversion of benzyl alcohol with a methoxy group (−OCH_3) at the para position is significantly higher than that of benzyl alcohol with Cl at the para position, which implies the corresponding reaction mechanism, as discussed in detail below.

A set of control experiments with different reaction conditions have been performed to explore the potential mechanism of the photocatalytic reaction. As illustrated in Figure S10, with the hole scavenger (triethanolamine, TEOA) added to the photocatalytic reaction system, the generation of BAD is significantly restrained, indicating that the oxidation half reaction of BA is driven by holes. When adding carbon tetrachloride (CCl_4) as the electron scavenger, the output of BAD has increased but the output of H_2 is almost negligible, indicating that the reduction of H^+ is driven by electrons, and the elimination of electrons promotes the oxidation reaction. Moreover, the control experiments show almost no activity on the generation of
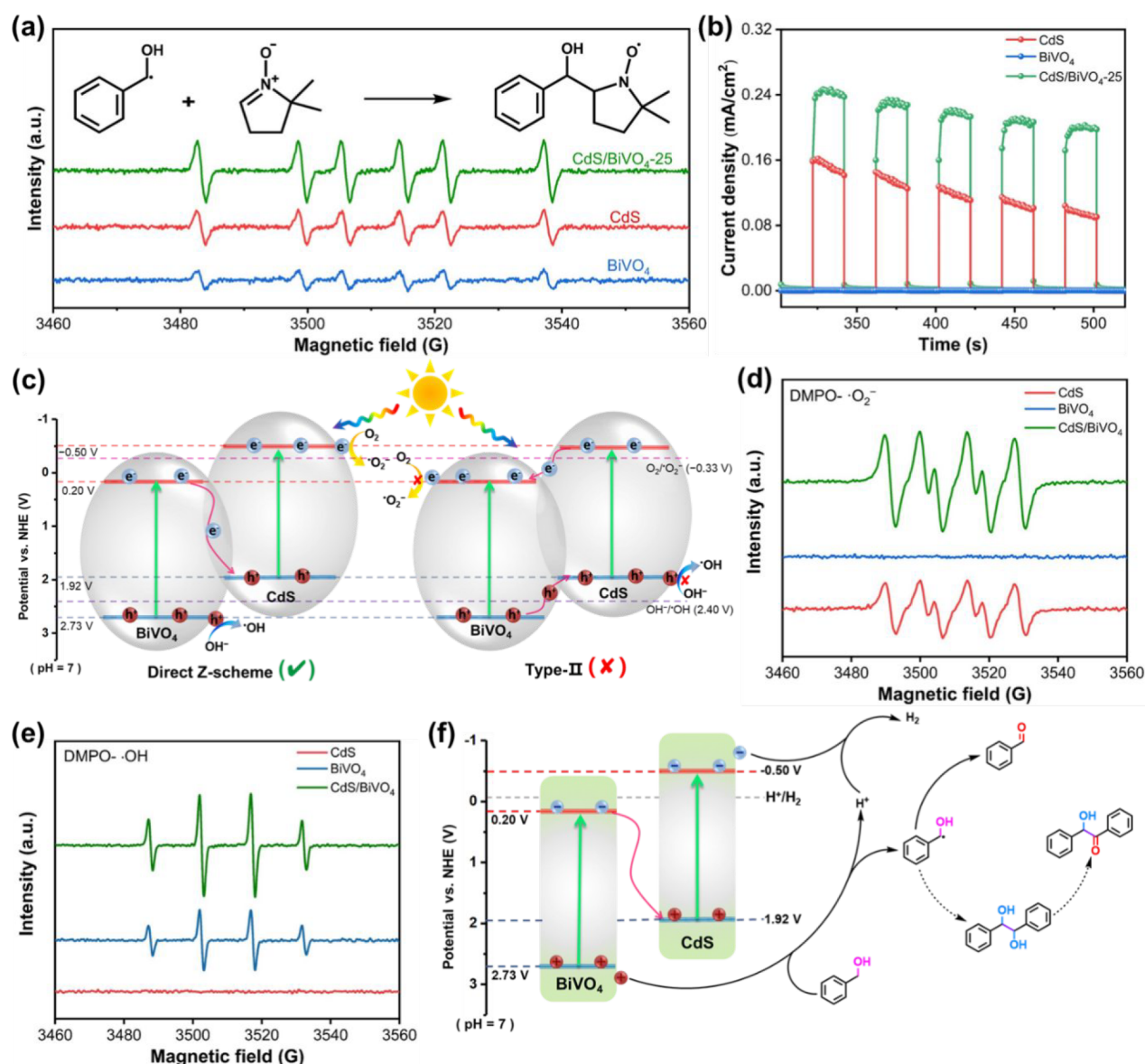
Figure 4. (a) EPR spectra of bare CdS, bare $BiVO_4$ and $CdS/BiVO_4$-25 with irradiation for 10 min. (b) Transient photocurrent−time (I−t) curves. (c) Schematic illustration of the migration pathway of photogenerated electrons and holes in accordance with type-II and direct Z-scheme system of the $CdS/BiVO_4$ hybrid. DMPO spin-trapping EPR images of bare CdS, $BiVO_4$, and $CdS/BiVO_4$ for DMPO-$^{\bullet}O_2^-$ (d) and DMPO-$^{\bullet}OH$ (e) under visible light irradiation. (f) Illustration of the band structure for $CdS/BiVO_4$ hybrids and the plausible reaction mechanism for the coupled reaction system of photocatalytic conversion of BA.

BAD and H_2 in the absence of visible light irradiation or photocatalyst, strongly proving that the reaction is a photocatalytic process driven by visible light. In addition, adding 5,5-dimethyl-1-pyrroline-N-oxide (DMPO) causes the conversion rate of BA to drop sharply, implying that the active species in the reaction is the carbon-center free radical.[16]

To gain insight into the information of the radical intermediates mechanism in the photocatalytic redox process, the electron paramagnetic resonance (EPR) technique was conducted to detect the free radicals in the reaction using DMPO as the trapping agent. As sketched in Figure 4a, no free radical signal appears in the dark, but six characteristic signal peaks with similar intensity at g = 2.0063 appear in all three samples under exposure to visible light. The result of a quantitative analysis for the above-mentioned EPR spectra suggests that the value of α_H = 22.7 and α_N = 16.0 (Figure S11) belong to $^{\bullet}CH(OH)Ph$ intermediates.[58,59] It is noteworthy that

the characteristic peaks intensity follows the $CdS/BiVO_4$ hybrid > bare CdS > bare $BiVO_4$, which is in line with the law of reaction activity.

A set of photoelectrochemical measurements have been carried out to unveil the origin of the significantly enhanced photoactivity of the $CdS/BiVO_4$ composites. The transient photocurrent responses analysis in Figure 4b display that the $CdS/BiVO_4$ hybrid has a significantly improved photocurrent response compared to bare CdS and $BiVO_4$, indicating that the recombination of photoinduced charge carriers has been significantly suppressed.[60] The linear sweep voltammetry (LSV) curves (Figure S12) suggest that the $CdS/BiVO_4$ hybrid has a higher current density at a similar potential range, proving that the formation of heterostructures effectively enhances charge transfer.[61] Besides, the electrochemical impedance spectroscopy (EIS) has been utilized to study the inhibition of charge migration between the electrolyte and the sample. As

depicted in Figure S13, the CdS/BiVO$_4$ composite has the smallest arc radius at high frequency, which proves that it can more effectively promote the migration of photoexcited charges relative to the bare CdS and BiVO$_4$.[60] Photoluminescence (PL) measurement was performed to in-depth study the behavior of photogenerated carriers. As exemplified in Figure S14, the PL intensity of the CdS/BiVO$_4$ hybrid is significantly quenched under 380 nm excitation, confirming that the formation of the heterostructure effectively hinders the recombination of photoexcited electron−hole pairs. As mentioned above, the construction of the CdS/BiVO$_4$ heterostructure effectively promotes the separation and transfer of photoexcited electron−hole pairs, thereby improving the photocatalytic performance of the composite.

Taking into account the energy band structure of CdS and BiVO$_4$, there are two possibilities for the charge carrier migration path existing in our photocatalytic system: traditional type-II heterojunction and direct Z-scheme system (Figure 4c). Given the respective CB positions of CdS and BiVO$_4$, it is obvious that the CB position of BiVO$_4$ is too low to drive protons reduction. Furthermore, the dominant oxidation product of BA over the optimal catalyst is BAD, indicating that the oxidation reaction is concentrated on the surface of BiVO$_4$ NSs. EPR spin-trapping has been conducted to further verify the Z-scheme charge transfer mechanism.[62] Under the condition of adding different catalysts, DMPO is deployed to trap $^{\bullet}O_2^-$ and $^{\bullet}OH$ in methanol solution and aqueous solution, respectively. Since the energy level of the $O_2/^{\bullet}O_2^-$ couple (−0.33 V) is more positive than the CB of CdS but more negative than the CB of BiVO$_4$, only CdS can reduce O_2 into $^{\bullet}O_2^-$ ($O_2 + e^- \rightarrow {}^{\bullet}O_2^-$). Analogously, the energy level of the $OH^-/^{\bullet}OH$ couple (2.40 V) is more positive than the VB of CdS but more negative than BiVO$_4$, suggesting that only BiVO$_4$ can oxidize H_2O into $^{\bullet}OH$ ($OH^- + h^+ \rightarrow {}^{\bullet}OH$). As depicted in Figure 4d,e, after visible irradiation for a while, DMPO-$^{\bullet}O_2^-$ is detected only in the samples of bare CdS or CdS/BiVO$_4$ hybrid, and DMPO-$^{\bullet}OH$ is only detected when present in the samples of bare BiVO$_4$ or CdS/BiVO$_4$ hybrid. Obviously, the signal peaks of CdS/BiVO$_4$ hybrid are significantly higher than that of CdS or BiVO$_4$. The above results indicate that the photoexcited electrons and holes are effectively separated and respectively concentrated in CdS and BiVO$_4$, thereby evidently confirming a direct Z-scheme charge transfer mechanism, instead of a conventional type-II charge transfer mechanism, in our photocatalytic system.

Combining the aforementioned analyses, an underlying photocatalytic mechanism for the selective conversion of BA to BAD and H_2 over the CdS/BiVO$_4$ hybrid is proposed as follows (Figure 4f). Initially, both CdS and BiVO$_4$ generate photoexcited electron−hole pairs under visible light illumination ($\lambda > 420$ nm). Owing to the ultrathin thickness of BiVO$_4$ NSs and the close interfacial contact between CdS NRs and BiVO$_4$ NSs, the photogenerated electrons on the CB of BiVO$_4$ quickly transfer to the surface, and further migrate to the VB of CdS to recombine with the photogenerated holes, thereby realizing the effective separation of photoexcited electron−hole pairs. In this case, the electrons and holes of the composite accumulate in the CB of CdS and the VB of BiVO$_4$, respectively, thereby maintaining a strong reduction and oxidation ability. Afterward, the hydrogen atom in α-C−H of BA can be abstracted and separated by photoexcited holes to form H^+ and $^{\bullet}CH(OH)Ph$ intermediates. These dropped H^+ are quickly reduced by the electrons accumulated in the CB of the nearby

CdS NRs, thereby generating H_2. Meanwhile, the $^{\bullet}CH(OH)Ph$ intermediates can be further oxidized to BAD, or C−C coupling products due to its instability. Notably, benzylic alcohols with electron-donating groups at the para position are apt to be attracted by holes due to the greater electron density, so that the hydrogen atoms in α-C−H are more likely to shed off. Consequently, benzylic alcohols with electron-donating groups exhibit significantly enhanced conversion, and conversely, benzylic alcohols with electron-withdrawing groups exhibit significantly decreased conversion.

4. CONCLUSION

In summary, we have successfully synthesized 1D/2D CdS NRs/BiVO$_4$ NSs binary composites through a facile electrostatic self-assembly approach for the selective oxidation of BA accompanied by H_2 evolution under visible light irradiation. Compared with bare CdS and bare BiVO$_4$, the construction of the Z-scheme heterostructure remarkably hinders the recombination of photogenerated charge carriers and retains strong redox ability in the meantime. The photocatalytic activity over the CdS/BiVO$_4$ hybrid is greatly enhanced toward merging BAD production and H_2 evolution in comparison with that over bare CdS and BiVO$_4$. It is anticipated that the semiconductor-based composite photocatalysts with a Z-scheme heterostructure exhibit promising potential in such dual-function photoredox systems, which can effectively utilize photogenerated holes and electrons to produce clean fuels and fine chemicals with high added value.

■ ASSOCIATED CONTENT

Ⓢ Supporting Information

The Supporting Information is available free of charge at https://pubs.acs.org/doi/10.1021/acsphyschemau.1c00053.

> Methods for the synthesis and characterization of catalysts, specific process, and results of the recycling tests, EDX spectrum of CdS/BiVO$_4$, estimated band gap energy of CdS and BiVO$_4$, Mott−Schottky plots, survey XPS spectrum, mass spectrogram, XRD patterns before and after cyclic tests, results of control experiments, quantitative analysis result of EPR spectrum, polarization curves, EIS Nyquist plots, PL spectra and results of extended experiments (PDF)

■ AUTHOR INFORMATION

Corresponding Authors

Zi-Rong Tang − *College of Chemistry, State Key Laboratory of Photocatalysis on Energy and Environment, Fuzhou University, Fuzhou, Fujian 350116, P. R. China;* ⓞ orcid.org/0000-0002-6564-3539; Email: zrtang@ fzu.edu.cn

Yi-Jun Xu − *College of Chemistry, State Key Laboratory of Photocatalysis on Energy and Environment, Fuzhou University, Fuzhou, Fujian 350116, P. R. China;* ⓞ orcid.org/0000-0002-2195-1695; Email: yjxu@ fzu.edu.cn

Authors

Feng-Kang Shang − *College of Chemistry, State Key Laboratory of Photocatalysis on Energy and Environment, Fuzhou University, Fuzhou, Fujian 350116, P. R. China*

Ming-Yu Qi − *College of Chemistry, State Key Laboratory of Photocatalysis on Energy and Environment, Fuzhou University, Fuzhou, Fujian 350116, P. R. China*

Chang-Long Tan − *College of Chemistry, State Key Laboratory of Photocatalysis on Energy and Environment, Fuzhou University, Fuzhou, Fujian 350116, P. R. China*

Complete contact information is available at:
https://pubs.acs.org/10.1021/acsphyschemau.1c00053

Notes

The authors declare no competing financial interest.

■ REFERENCES

(1) Tan, C.-L.; Qi, M.-Y.; Tang, Z.-R.; Xu, Y.-J. Cocatalyst decorated ZnIn$_2$S$_4$ composites for cooperative alcohol conversion and H$_2$ evolution. *Appl. Catal., B* **2021**, *298*, 120541.

(2) Yang, M.-Q.; Xu, Y.-J. Selective photoredox using graphene-based composite photocatalysts. *Phys. Chem. Chem. Phys.* **2013**, *15* (44), 19102−19118.

(3) She, H.; Zhou, H.; Li, L.; Wang, L.; Huang, J.; Wang, Q. Nickel-Doped Excess Oxygen Defect Titanium Dioxide for Efficient Selective Photocatalytic Oxidation of Benzyl Alcohol. *ACS Sustainable Chem. Eng.* **2018**, *6* (9), 11939−11948.

(4) Zheng, C.; He, G.; Xiao, X.; Lu, M.; Zhong, H.; Zuo, X.; Nan, J. Selective photocatalytic oxidation of benzyl alcohol into benzaldehyde with high selectivity and conversion ratio over Bi$_4$O$_5$Br$_2$ nanoflakes under blue LED irradiation. *Appl. Catal., B* **2017**, *205*, 201−210.

(5) Zhong, L.; Mao, B.; Liu, M.; Liu, M.; Sun, Y.; Song, Y.-T.; Zhang, Z.-M.; Lu, T.-B. Construction of hierarchical photocatalysts by growing ZnIn$_2$S$_4$ nanosheets on Prussian blue analogue-derived bimetallic sulfides for solar co-production of H$_2$ and organic chemicals. *J. Energy Chem.* **2021**, *54*, 386−394.

(6) Li, J.-Y.; Li, Y.-H.; Qi, M.-Y.; Lin, Q.; Tang, Z.-R.; Xu, Y.-J. Selective Organic Transformations over Cadmium Sulfide-Based Photocatalysts. *ACS Catal.* **2020**, *10* (11), 6262−6280.

(7) Zhang, N.; Ciriminna, R.; Pagliaro, M.; Xu, Y.-J. Nanochemistry-derived Bi$_2$WO$_6$ nanostructures: towards production of sustainable chemicals and fuels induced by visible light. *Chem. Soc. Rev.* **2014**, *43* (15), 5276−5287.

(8) Magdziarz, A.; Colmenares, J. C.; Chernyayeva, O.; Kurzydlowski, K.; Grzonka, J. Iron-Containing Titania Photocatalyst Prepared by the Sonophotodeposition Method for the Oxidation of Benzyl Alcohol. *ChemCatChem.* **2016**, *8* (3), 536−539.

(9) Giannakoudakis, D. A.; Qayyum, A.; Nair, V.; Khan, A.; Pradhan, S. R.; Prekodravac, J.; Rekos, K.; LaGrow, A. P.; Bondarchuk, O.; Lomot, D.; Triantafyllidis, K. S.; Colmenares, J. C. Ultrasound-assisted decoration of CuO$_x$ nanoclusters on TiO$_2$ nanoparticles for additives free photocatalytic hydrogen production and biomass valorization by selective oxidation. *Mol. Catal.* **2021**, *514*, 111664.

(10) Khan, A.; Goepel, M.; Lisowski, W.; Lisovytskiy, D.; Mazurkiewicz-Pawlicka, M.; Glaser, R.; Colmenares, J. C. Titania/chitosan-lignin nanocomposite as an efficient photocatalyst for the selective oxidation of benzyl alcohol under UV and visible light. *RSC Adv.* **2021**, *11* (55), 34996−35010.

(11) Shen, Z.; Hu, Y.; Li, B.; Zou, Y.; Li, S.; Busser, G. W.; Wang, X.; Zhao, G.; Muhler, M. State-of-the-art progress in the selective photooxidation of alcohols. *J. Energy Chem.* **2021**, *62*, 338−350.

(12) Zhang, N.; Liu, S.; Fu, X.; Xu, Y.-J. Fabrication of coenocytic Pd@CdS nanocomposite as a visible light photocatalyst for selective transformation under mild conditions. *J. Mater. Chem.* **2012**, *22* (11), 5042−5052.

(13) Han, C.; Tang, Z.-R.; Liu, J.; Jin, S.; Xu, Y.-J. Efficient photoredox conversion of alcohol to aldehyde and H$_2$ by heterointerface engineering of bimetal-semiconductor hybrids. *Chem. Sci.* **2019**, *10* (12), 3514−3522.

(14) Luo, N.; Montini, T.; Zhang, J.; Fornasiero, P.; Fonda, E.; Hou, T.; Nie, W.; Lu, J.; Liu, J.; Heggen, M.; Lin, L.; Ma, C.; Wang, M.; Fan, F.; Jin, S.; Wang, F. Visible-light-driven coproduction of diesel precursors and hydrogen from lignocellulose-derived methylfurans. *Nat. Energy* **2019**, *4* (7), 575−584.

(15) Qi, M.-Y.; Conte, M.; Anpo, M.; Tang, Z.-R.; Xu, Y.-J. Cooperative Coupling of Oxidative Organic Synthesis and Hydrogen Production over Semiconductor-Based Photocatalysts. *Chem. Rev.* **2021**, *121* (21), 13051−13085.

(16) Lin, Q.; Li, Y.-H.; Qi, M.-Y.; Li, J.-Y.; Tang, Z.-R.; Anpo, M.; Yamada, Y. M. A.; Xu, Y.-J. Photoredox dual reaction for selective alcohol oxidation and hydrogen evolution over nickel surface-modified ZnIn$_2$S$_4$. *Appl. Catal., B* **2020**, *271*, 118946.

(17) Cui, Z.; Zhou, H.; Wang, G.; Zhang, Y.; Zhang, H.; Zhao, H. Enhancement of the visible-light photocatalytic activity of CeO$_2$ by chemisorbed oxygen in the selective oxidation of benzyl alcohol. *New J. Chem.* **2019**, *43* (19), 7355−7362.

(18) Shang, J.; Hao, W.; Lv, X.; Wang, T.; Wang, X.; Du, Y.; Dou, S.; Xie, T.; Wang, D.; Wang, J. Bismuth Oxybromide with Reasonable Photocatalytic Reduction Activity under Visible Light. *ACS Catal.* **2014**, *4* (3), 954−961.

(19) Li, X.-H.; Wang, X.; Antonietti, M. Solvent-Free and Metal-Free Oxidation of Toluene Using O$_2$ and g-C$_3$N$_4$ with Nanopores: Nanostructure Boosts the Catalytic Selectivity. *ACS Catal.* **2012**, *2* (10), 2082−2086.

(20) Yu, X.; Li, H.; Hao, X.; Zhang, Z.; Wang, Y.; Li, J.; Wang, K. Selective Oxidation of Benzyl Alcohol by Ag/Pd/m-BiVO$_4$ Microspheres under Visible Light Irradiation. *Catalysts* **2020**, *10* (2), 266.

(21) Tao, X.; Shao, L.; Wang, R.; Xiang, H.; Li, B. Synthesis of BiVO$_4$ nanoflakes decorated with AuPd nanoparticles as selective oxidation photocatalysts. *J. Colloid Interface Sci.* **2019**, *541*, 300−311.

(22) Jin, X.; Li, R.; Zhao, Y.; Liu, X.; Wang, X.; Jiao, H.; Li, J. Spatial separation of dual-cocatalysts on bismuth vanadate for selective aerobic oxidation of benzylalcohols to benzaldehydes under visible light irradiation. *Catal. Sci. Technol.* **2018**, *8* (23), 6173−6179.

(23) Qi, M.-Y.; Li, Y.-H.; Anpo, M.; Tang, Z.-R.; Xu, Y.-J. Efficient Photoredox-Mediated C-C Coupling Organic Synthesis and Hydrogen Production over Engineered Semiconductor Quantum Dots. *ACS Catal.* **2020**, *10* (23), 14327−14335.

(24) Wu, B.; Zhang, L.; Jiang, B.; Li, Q.; Tian, C.; Xie, Y.; Li, W.; Fu, H. Ultrathin Porous Carbon Nitride Bundles with an Adjustable Energy Band Structure toward Simultaneous Solar Photocatalytic Water Splitting and Selective Phenylcarbinol Oxidation. *Angew. Chem., Int. Ed.* **2021**, *60* (9), 4815−4822.

(25) Yu, Q.; Tang, Z.-R.; Xu, Y.-J. Synthesis of BiVO$_4$ nanosheets-graphene composites toward improved visible light photoactivity. *J. Energy Chem.* **2014**, *23* (5), 564−574.

(26) Wang, Y.; Tan, G.; Liu, T.; Su, Y.; Ren, H.; Zhang, X.; Xia, A.; Lv, L.; Liu, Y. Photocatalytic properties of the g-C$_3$N$_4$/{010} facets BiVO$_4$ interface Z-Scheme photocatalysts induced by BiVO$_4$ surface heterojunction. *Appl. Catal., B* **2018**, *234*, 37−49.

(27) Tan, H. L.; Tahini, H. A.; Wen, X.; Wong, R. J.; Tan, X.; Iwase, A.; Kudo, A.; Amal, R.; Smith, S. C.; Ng, Y. H. Interfacing BiVO$_4$ with Reduced Graphene Oxide for Enhanced Photoactivity: A Tale of Facet Dependence of Electron Shuttling. *Small* **2016**, *12* (38), 5295−5302.

(28) Hu, J.; Chen, W.; Zhao, X.; Su, H.; Chen, Z. Anisotropic Electronic Characteristics, Adsorption, and Stability of Low-Index

BiVO$_4$ Surfaces for Photoelectrochemical Applications. *ACS Appl. Mater. Interfaces* **2018**, *10* (6), 5475−5484.

(29) Wei, Z.-H.; Wang, Y.-F.; Li, Y.-Y.; Zhang, L.; Yao, H.-C.; Li, Z.-J. Enhanced photocatalytic CO$_2$ reduction activity of Z-scheme CdS/BiVO$_4$ nanocomposite with thinner BiVO$_4$ nanosheets. *J. CO$_2$ Util.* **2018**, *28*, 15−25.

(30) Zou, L.; Wang, H.; Wang, X. High Efficient Photodegradation and Photocatalytic Hydrogen Production of CdS/BiVO$_4$ Heterostructure through Z-Scheme Process. *ACS Sustainable Chem. Eng.* **2017**, *5* (1), 303−309.

(31) Chen, F.; Yang, Q.; Li, X.; Zeng, G.; Wang, D.; Niu, C.; Zhao, J.; An, H.; Xie, T.; Deng, Y. Hierarchical assembly of graphene-bridged Ag$_3$PO$_4$/Ag/BiVO$_4$ (040) Z-scheme photocatalyst: An efficient, sustainable and heterogeneous catalyst with enhanced visible-light photoactivity towards tetracycline degradation under visible light irradiation. *Appl. Catal., B* **2017**, *200*, 330−342.

(32) Gao, X.; Wu, H. B.; Zheng, L.; Zhong, Y.; Hu, Y.; Lou, X. W. Formation of Mesoporous Heterostructured BiVO$_4$/Bi$_2$S$_3$ Hollow Discoids with Enhanced Photoactivity. *Angew. Chem., Int. Ed.* **2014**, *53* (23), 5917−5921.

(33) He, Z.; Shi, Y.; Gao, C.; Wen, L.; Chen, J.; Song, S. BiOCl/BiVO$_4$ p-n Heterojunction with Enhanced Photocatalytic Activity under Visible-Light Irradiation. *J. Phys. Chem. C* **2014**, *118* (1), 389−398.

(34) Lopes, O. F.; Carvalho, K. T. G.; Avansi, W., Jr.; Ribeiro, C. Growth of BiVO$_4$ Nanoparticles on a Bi$_2$O$_3$ Surface: Effect of Heterojunction Formation on Visible Irradiation-Driven Catalytic Performance. *J. Phys. Chem. C* **2017**, *121* (25), 13747−13756.

(35) Maeda, K. Z-Scheme Water Splitting Using Two Different Semiconductor Photocatalysts. *ACS Catal.* **2013**, *3* (7), 1486−1503.

(36) Li, H.; Tu, W.; Zhou, Y.; Zou, Z. Z-Scheme Photocatalytic Systems for Promoting Photocatalytic Performance: Recent Progress and Future Challenges. *Adv. Sci.* **2016**, *3* (11), 1500389.

(37) Zhou, F. Q.; Fan, J. C.; Xu, Q. J.; Min, Y. L. BiVO$_4$ nanowires decorated with CdS nanoparticles as Z-scheme photocatalyst with enhanced H$_2$ generation. *Appl. Catal., B* **2017**, *201*, 77−83.

(38) Han, B.; Liu, S.; Xu, Y.-J.; Tang, Z.-R. 1D CdS nanowire-2D BiVO$_4$ nanosheet heterostructures toward photocatalytic selective fine-chemical synthesis. *RSC Adv.* **2015**, *5* (21), 16476−16483.

(39) Li, Y.-H.; Zhang, F.; Chen, Y.; Li, J.-Y.; Xu, Y.-J. Photoredox-catalyzed biomass intermediate conversion integrated with H$_2$ production over Ti$_3$C$_2$T$_x$/CdS composites. *Green Chem.* **2020**, *22* (1), 163−169.

(40) Ma, D.; Shi, J.-W.; Sun, L.; Sun, Y.; Mao, S.; Pu, Z.; He, C.; Zhang, Y.; He, D.; Wang, H.; Cheng, Y. Knack behind the high performance CdS/ZnS-NiS nanocomposites: Optimizing synergistic effect between cocatalyst and heterostructure for boosting hydrogen evolution. *Chem. Eng. J.* **2022**, *431*, 133446.

(41) Sun, G.; Shi, J.-W.; Mao, S.; Ma, D.; He, C.; Wang, H.; Cheng, Y. Dodecylamine coordinated tri-arm CdS nanorod wrapped in intermittent ZnS shell for greatly improved photocatalytic H$_2$ evolution. *Chem. Eng. J.* **2022**, *429*, 132382.

(42) Sun, G.; Xiao, B.; Zheng, H.; Shi, J.-W.; Mao, S.; He, C.; Li, Z.; Cheng, Y. Ascorbic acid functionalized CdS-ZnO core-shell nanorods with hydrogen spillover for greatly enhanced photocatalytic H$_2$ evolution and outstanding photostability. *J. Mater. Chem. A* **2021**, *9* (15), 9735−9744.

(43) Sun, G.; Xiao, B.; Shi, J.-W.; Mao, S.; He, C.; Ma, D.; Cheng, Y. Hydrogen spillover effect induced by ascorbic acid in CdS/NiO core-shell p-n heterojunction for significantly enhanced photocatalytic H$_2$ evolution. *J. Colloid Interface Sci.* **2021**, *596*, 215−224.

(44) Gao, P.; Liu, J.; Lee, S.; Zhang, T.; Sun, D. D. High quality graphene oxide-CdS-Pt nanocomposites for efficient photocatalytic hydrogen evolution. *J. Mater. Chem.* **2012**, *22* (5), 2292−2298.

(45) Gao, X.-F.; Sun, W.-T.; Hu, Z.-D.; Ai, G.; Zhang, Y.-L.; Feng, S.; Li, F.; Peng, L.-M. An Efficient Method To Form Heterojunction CdS/TiO$_2$ Photoelectrodes Using Highly Ordered TiO$_2$ Nanotube Array Films. *J. Phys. Chem. C* **2009**, *113* (47), 20481−20485.

(46) Li, R.; Chen, H.; Xiong, J.; Xu, X.; Cheng, J.; Liu, X.; Liu, G. A Mini Review on Bismuth-Based Z-Scheme Photocatalysts. *Mater.* **2020**, *13* (22), 5057.

(47) Nie, Q. L.; Yuan, Q. L.; Chen, W. X.; Xu, Z. D. Effects of coordination agents on the morphology of CdS nanocrystallites synthesized by the hydrothermal method. *J. Cryst. Growth* **2004**, *265* (3−4), 420−424.

(48) Zhu, R.; Yang, R.; Hu, L.; Chen, B. Preparation of Z-Scheme system of CdS-RGO-BiVO$_4$ and its activity for hydrogen production. *Int. J. Hydrogen Energy* **2019**, *44* (36), 25119−25128.

(49) Li, J.-Y.; Li, Y.-H.; Zhang, F.; Tang, Z.-R.; Xu, Y.-J. Visible-light-driven integrated organic synthesis and hydrogen evolution over 1D/2D CdS-Ti$_3$C$_2$T$_x$ MXene composites. *Appl. Catal., B* **2020**, *269*, 118783.

(50) Liu, S.; Xu, Y.-J. Efficient electrostatic self-assembly of one-dimensional CdS-Au nanocomposites with enhanced photoactivity, not the surface plasmon resonance effect. *Nanoscale* **2013**, *5* (19), 9330−9339.

(51) Sun, Z.; Liu, X.; Yue, Q.; Jia, H.; Du, P. Cadmium Sulfide Nanorods Decorated with Copper Sulfide via One-Step Cation Exchange Approach for Enhanced Photocatalytic Hydrogen Evolution under Visible Light. *ChemCatChem.* **2016**, *8* (1), 157−162.

(52) Li, R.; Zhang, F.; Wang, D.; Yang, J.; Li, M.; Zhu, J.; Zhou, X.; Han, H.; Li, C. Spatial separation of photogenerated electrons and holes among {010} and {110} crystal facets of BiVO$_4$. *Nat. Commun.* **2013**, *4* (1), 1432.

(53) Yu, Z. B.; Xie, Y. P.; Liu, G.; Lu, G. Q.; Ma, X. L.; Cheng, H.-M. Self-assembled CdS/Au/ZnO heterostructure induced by surface polar charges for efficient photocatalytic hydrogen evolution. *J. Mater. Chem. A* **2013**, *1* (8), 2773−2776.

(54) Zhang, L. J.; Li, S.; Liu, B. K.; Wang, D. J.; Xie, T. F. Highly Efficient CdS/WO$_3$ Photocatalysts: Z-Scheme Photocatalytic Mechanism for Their Enhanced Photocatalytic H$_2$ Evolution under Visible Light. *ACS Catal.* **2014**, *4* (10), 3724−3729.

(55) Balachandran, S.; Prakash, N.; Thirumalai, K.; Muruganandham, M.; Sillanpaa, M.; Swaminathan, M. Facile Construction of Heterostructured BiVO$_4$-ZnO and Its Dual Application of Greater Solar Photocatalytic Activity and Self-Cleaning Property. *Ind. Eng. Chem. Res.* **2014**, *53* (20), 8346−8356.

(56) Zhang, Y.; Guo, Y.; Duan, H.; Li, H.; Sun, C.; Liu, H. Facile synthesis of V^{4+} self-doped, 010 oriented BiVO$_4$ nanorods with highly efficient visible light-induced photocatalytic activity. *Phys. Chem. Chem. Phys.* **2014**, *16* (44), 24519−24526.

(57) Yun, S. H.; Ingole, P. G.; Choi, W. K.; Kim, J. H.; Lee, H. K. Synthesis of cross-linked amides and esters as thin film composite membrane materials yields permeable and selective material for water vapor/gas separation. *J. Mater. Chem. A* **2015**, *3* (15), 7888−7899.

(58) Meng, S.; Ning, X.; Chang, S.; Fu, X.; Ye, X.; Chen, S. Simultaneous dehydrogenation and hydrogenolysis of aromatic alcohols in one reaction system via visible-light-driven heterogeneous photocatalysis. *J. Catal.* **2018**, *357*, 247−256.

(59) Chao, Y.; Zhang, W.; Wu, X.; Gong, N.; Bi, Z.; Li, Y.; Zheng, J.; Zhu, Z.; Tan, Y. Visible-Light Direct Conversion of Ethanol to 1,1-Diethoxyethane and Hydrogen over a Non-Precious Metal Photocatalyst. *Chem.—Eur. J.* **2019**, *25* (1), 189−194.

(60) Jiang, C.; Wang, H.; Wang, Y.; Ji, H. All solid-state Z-scheme CeO$_2$/ZnIn$_2$S$_4$ hybrid for the photocatalytic selective oxidation of aromatic alcohols coupled with hydrogen evolution. *Appl. Catal., B* **2020**, *277*, 119235.

(61) Hao, X.; Cui, Z.; Zhou, J.; Wang, Y.; Hu, Y.; Wang, Y.; Zou, Z. Architecture of high efficient zinc vacancy mediated Z-scheme photocatalyst from metal-organic frameworks. *Nano Energy* **2018**, *52*, 105−116.

(62) Wang, Y.; Kong, X.; Jiang, M.; Zhang, F.; Lei, X. A Z-scheme ZnIn$_2$S$_4$/Nb$_2$O$_5$ nanocomposite: constructed and used as an efficient bifunctional photocatalyst for H$_2$ evolution and oxidation of 5-hydroxymethylfurfural. *Inorg. Chem. Front.* **2020**, *7* (2), 437−446.